Chapter 7

Microwave Plasmas as a Processing Tool for Tailoring the Surface Properties of Ceramic Coatings

Emmanuel J. Ekoi, Muhammad Awais and Denis P. Dowling

Additional information is available at the end of the chapter

http://dx.doi.org/10.5772/intechopen.71686

Abstract

This chapter reviews the use of low pressure microwave plasmas as a processing technology for both sintering and controlling the surface chemistry of porous ceramic coatings. A particular advantage of microwave processing is its ability to penetrate the surface of the workpiece; enabling rapid volumetric heating and thus reducing the need for external heat sources. The microwave plasma treatments have the ability to sinter materials in minutes rather than the hours taken using conventional furnace processing. This study provides examples of the use of these plasmas to sinter both nickel and titanium nanoparticles. These are used in the fabrication of electrodes for use in dye sensitized solar cells. Further applications of the microwave plasma treatments investigated is for their use in heat treatment to control crystalline phase transitions, as well as a rapid technique to oxidize metal surfaces.

Keywords: microwave plasma, porous ceramics, nickel oxide, titanium oxide, coatings

1. Introduction

Microwaves are electromagnetic waves with wavelengths from 1 mm to 1 m and corresponding frequencies between 0.3 MHz and 300 GHz [1, 2]. The use of microwave treatments (non-plasma), as an energy source for the heat treatment of metals, ceramics and composites has been reported to be more effective than conventional furnace heating methods, due to the improved microstructure and properties, reduction in processing time, etc. [1–3]. These microwave treatments are usually carried out at 0.915 GHz, 2.45 GHz and 20–30 GHz frequencies in agreement with the industrial, scientific and medical (ISM) radio bands set aside for non-communication purposes [2, 4]. During microwave processing, energy is supplied

by an electromagnetic field directly to the material by the interaction of the molecules of the material with electromagnetic field. In contrast, conventional thermal processing involves the transfer of energy by conduction, convection and radiation [5].

Clark et al. [1] reviewed the effectiveness of microwave heating and found it to be substrate material dependant. Materials were, thus, grouped into categories (depending on the electromagnetic field-material interaction) as: transparent (low dielectric loss materials); opaque (conductors); absorbing (high dielectric loss materials); and mixed absorbing where there is selective absorption due to differences in dielectric loss in the materials.

Several researchers have demonstrated the capability of using microwave to process metallic and ceramic materials [6–11]. It has been reported that a distinction in the microstructure and porosity distribution can be made between conventional and microwave sintered materials with respect to the pore shape. Microwave sintered samples exhibit pores with more rounded edges than the conventionally sintered materials. The sphericity of pore is reported to be critical in the ductility and strength of the sintered material [11].

In addition to the use of microwaves directly, a plasma discharge can also be formed using the microwave energy, if the appropriate conditions (gas type, pressure, resonator, etc.) are in place. Briefly by way of introduction to this technique, a plasma is described as a collection of unbound charged particles, photons and neutral atomic or molecular species which are electrically neutral on average [12, 13]. Plasma generation arises from the excitation and ionization of gases by energy transfer from various sources to the gases to form excited, charged and neutral species [14]. There are a range of plasma types including high frequency, DC and low frequency discharges [15, 16]. The latter include systems such as glow discharge, corona discharge, hollow cathode discharge [16], while the high frequency consists of radio frequency (RF) and microwave plasma discharges [17].

Microwave plasma systems are usually electrodeless systems and thus, differ from DC and RF systems which mostly use electrodes to generate plasma. In these systems, microwaves are usually guided using waveguide into the chamber where energy is impacted to the gas to form plasma by partially ionizing the gas [18, 19]. A typical example of microwave plasma system is the circumferential antenna plasma (CAP) microwave reactor, which operates at 2.45 GHz (**Figure 1**). In this CAP system, a cylindrical quartz ring window, 345 mm in diameter, embedded in the wall of the plasma chamber guides the microwaves into the plasma chamber. The microwaves are directed to the plasma chamber through a coaxial waveguide, and expands radially as it moves towards the cylindrical quartz ring window. A perfect rotational symmetry is obtained when the microwave which has uniform amplitude and phase distribution passes through the quartz window [20]. The cylindrical geometry of the configuration ensures that the formation of microwave power density at the window is lower than in the center of the chamber; thus, no plasma is formed adjacent to the window [21].

The use of microwave plasma source for surface and bulk treatment of metal and ceramics has the potential to be more effective than DC and RF plasmas, because of the higher density of active atomic species that can be generated using this type of discharge [22]. Microwave discharges generally have higher electron kinetic temperature and number density because

http://dx.doi.org/10.5772/intechopen.71686

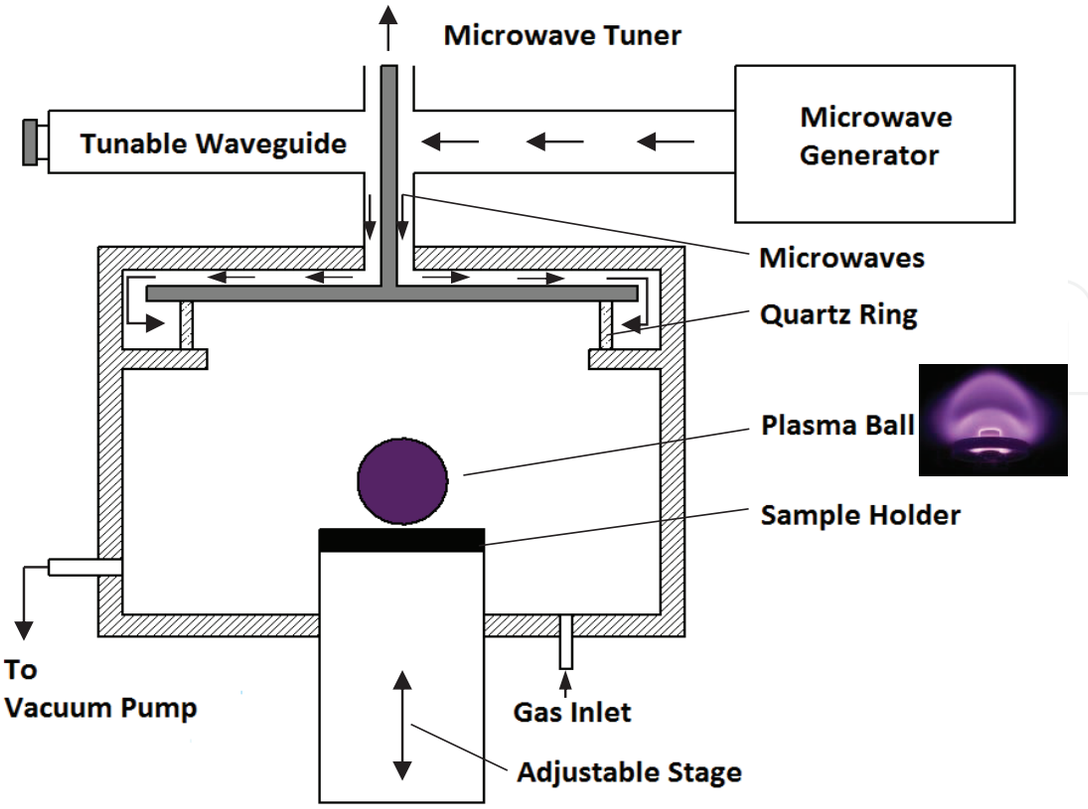

Figure 1. Schematic representation of CAP microwave plasma system.

the power is usually coupled through radiation and thus, bypasses sheath losses [17, 23]. A further advantage of these plasmas is that they can be operated in a wide gas pressure range [24, 25], which combine with the higher electron temperature generally obtained, makes them capable of providing a higher fraction of ionization and dissociation [24].

Metal oxide layers can be obtained using a range of techniques including sol-gel, hydrothermal synthesis, electrophoretic deposition, sputtering, electrochemical treatments (anodic oxidation), chemical vapor deposition (CVD), physical vapor deposition and ion implantation, etc. [26–32]. Most of the techniques (except sputtering and direct metal oxide growth on metal surfaces) require sintering to enhance the packing density, porosity and the adhesion of the deposited coatings. A range of characterisation techniques usually applied includes a FEI Quanta 3D FEG DualBeam scanning electron microscope (SEM) (Morphology); a focused ion beam (FIB)(Thickness); Energy-dispersive X-ray spectroscopy (EDX) (Elemental data); Veeco NT1100 optical profilometer (Surface roughness). Siemens D500 XRD system (Phase identification), a LASCON QP003 and LPC03 ratio pyrometers from Dr. Mergenthaler GmbH & Co. KG. (Temperature measurements) and a J.A. Woollam ellipsometer with a Tauc-Lorentz fitting via completeEASE® software (Band gap and coating thickness).

Having provided an introduction to microwave plasma treatments along with the associated characterization techniques, the following sections firstly provide an overview of the use of microwave plasmas for the sintering of metal oxide powders. The use of microwave plasma treatments for sintering, has previously been described as rapid discharge sintering (RDS).

The specific focus is on the sintering of nanoparticles of nickel oxide (NiO) and titanium dioxide (TiO_2), used as electrodes in dye sensitized solar cells (DSSCs). The effect of the plasma treatments on thermal sensitive crystalline phase changes, is also discussed. A further application reported is that of the use of microwave plasma treatments for the oxidation of metal surfaces, in order to produce porous oxide ceramic (TiO_2) layers on the metal surface.

2. Microwave plasma sintering of nanoparticles

Considerable research has been carried out to understand the interaction of microwave radiation with materials [33, 34]. The ability of microwaves to penetrate work pieces enables volumetric heating at a rapid rate, thus avoiding the need of external heat sources [33]; this makes it an attractive technique in material processing. However, poor coupling in non-plasma microwave processing may result in a non-uniform heating of the substrates [35]. One of the advantages of microwave plasma treatment is the combined advantage inherent in microwave and plasma heating in terms of volumetric, homogeneous and rapid heating [2, 36, 37]. For example, the work of Twomey et al. [37] demonstrates that homogenous heating of substrates could be achieved using microwave plasma treatments including considerably lower cycle times [38] compared to non-plasma microwave and furnace heating. In this section, the use of microwave plasma processing for the sintering of Nickel oxide (NiO) and Titanium dioxide (TiO_2) particles is presented.

2.1. Sintering of nickel oxide (NiO) nanoparticles

NiO coatings are used extensively as a photocathode in the construction of *p*-type DSSCs [39–42] due to their *p*-type semiconductivity [43], and well defined electrical and optical properties [44]. Furthermore, its bandgap energy which range from 3.6 to 4.0 eV helps to make it a model semiconductor substrate [43]. Also, it is considered a good electron donor for numerous photo sensitizers due to its valance bond potential; thus, the NiO coatings are readily quenched with many dye sensitizers [45]. In this section, the use of microwave plasma processing for the sintering of NiO particles to produce coatings for use in DSSC electrodes is discussed [42, 46].

2.1.1. Rapid discharge sintering vs. conventional furnace sintering

In order to process NiO using the RDS technique, a spray technique is used to deposit solvent slurry of NiO nanoparticles onto conductive glass substrates (**Figure 2**). The spray technique involves suspending the NiO nanoparticles in alcohol; the mixture is then applied via spraying onto fluorine-doped tin oxide (FTO) coated glass substrates to form the coating. A subsequent step is carried out after spraying in order to enhance the interconnectivity between the NiO particles by sintering, as well as an increased level of adhesion to the conductive glass substrate. This sintering step was investigated using both microwave plasma and furnace treatments [42, 46]. The latter was carried out using a CWF 1200 Carbolite tube air furnace. Typical furnace sintering temperatures in the range of 300–450°C have been reported

http://dx.doi.org/10.5772/intechopen.71686

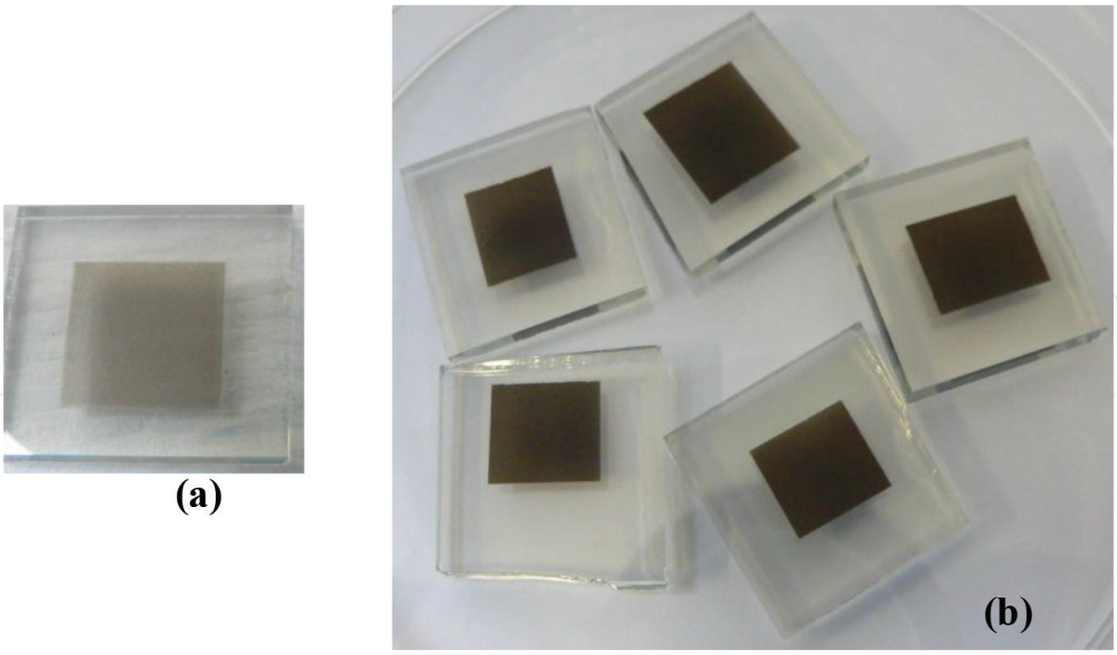

Figure 2. (a) 0.6 (b) 2.5 μm thick NiO coatings deposited using spray technique.

previously [47–51]. In this study, a treatment temperature of approximately 450°C was used for a 5-min period for both the furnace and RDS treatments. This treatment time was chosen because it yielded the best photovoltaic performance for RDS treatment. Overall, a cycle time of ~120 min was required for the furnace sintering including heat up, maintenance at the max 450°C temperature and cool down. In contrast, the RDS processing required only 15 min, included all stages such as pump down, plasma treatment, and cooling.

In this Section, the properties of the furnace sintered coatings, such as morphology, crystal structure, dye adsorption, chemical composition and photovoltaic performance are compared with the NiO coatings treated for 5 min, using the RDS technique.

2.1.1.1. Morphological analyses of porous NiO coatings

A typical SEM micrograph of the morphology of RDS and furnace treated coatings is given in **Figure 3**. A higher level of interconnectivity with reduced grain growth for the RDS treated coatings when compared with the furnace sintered coatings can be observed. The increased grain growth in the furnace sintered coatings could be due to a slower cooling rate (10°C/min) used in the furnace process. In contrast, the RDS technique requires only a 5-min cooling time following the plasma treatment.

A further examination of NiO coatings using an FIB/SEM cross section micrograph (**Figure 4**) indicated that the RDS treated coating displays an improved level of porosity as well as interfacial connection between the NiO coating and FTO substrate. This could be due to the difference in the type of heating mechanisms in both sintering techniques. RDS treatment encompasses volumetric heating, which delivers more efficient heating inside the NiO coating matrix than that obtained with furnace sintering where a conductive type of heating is

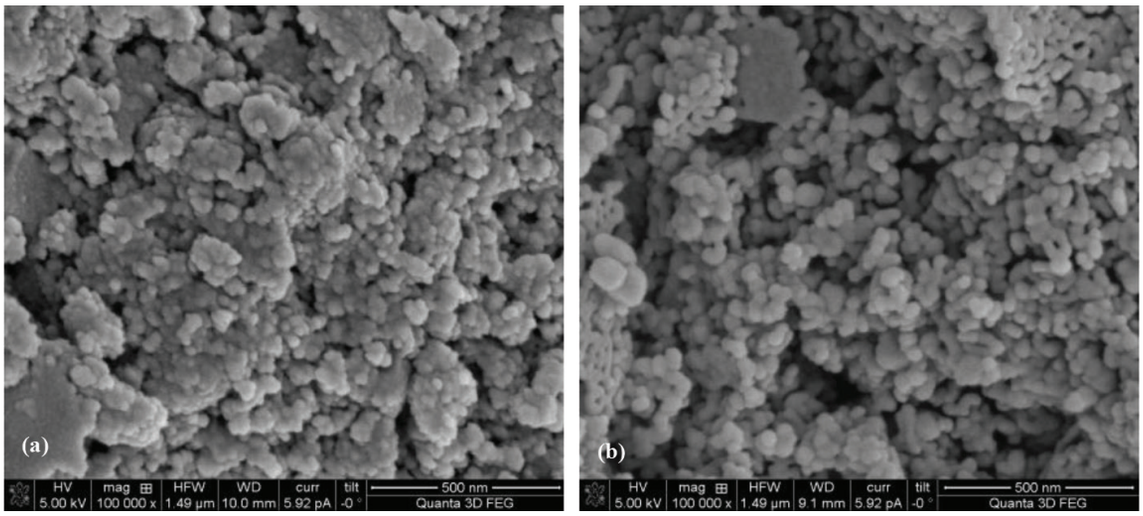

Figure 3. SEM images of ~2.5 μm thick NiO coatings treated using (a) RDS (b) furnace sintering [52].

present. Also, furnace sintering could have resulted in inhomogeneous heating of coatings' surface to yield a heat affected zone [53]; thus, a more open structure is observed for the RDS treated coatings when compared with the furnace sintered samples.

2.1.1.2. Crystal structure, crystallite size and dye adsorption evaluations of NiO coatings

As shown in **Figure 3**, the NiO grain size obtained using the RDS process was smaller than that obtained after treatment using the furnace. A measurement of the crystallite size of NiO coatings obtained using similar sintering techniques to **Figure 3** indicated that the sizes were approximately 6.5 and 14.0 nm, respectively [42]. Thus, the RDS technique results in a finer grain size, in addition to a more uniform heating/sintering of the NiO nanoparticles.

The effect of a smaller grain size and a more open structure (**Figures 3** and **4**) obtained using the RDS technique may be observed in the UV-vis absorption spectra of the NiO coatings obtained using the two sintering techniques (**Figure 5**). The level of dye adsorption increased up to 44% for the case of RDS treated NiO coatings when compared with the furnace sintered coatings of the same thickness.

2.1.1.3. Comparison of photovoltaic performance of porous NiO coatings

Another parameter which can be used to portray the performance of the porous NiO structure is its photovoltaic performance (*I-V* characteristic) when evaluated as part of a *p*-type DSSCs. A comparison of the photovoltaic performance of NiO coatings prepared by various researchers is given in **Table 1**. From this Table, it is clear that the light-to-current conversion efficiency increase of almost 10-fold for the RDS treated NiO coatings (1–2 μm and 2.5 μm thick), when compared with the furnace sintered coatings. The conversion efficiency of the furnace treated coatings (1–2 μm thick) is comparable to the values reported in the literature [42, 46]. A notable observation is that a 2.5 μm thick NiO coatings, prepared using the RDS treatment, exhibited the best performance; it is likely due to improved dye adsorption with enhanced active sites, which results in better photochemical reaction.

http://dx.doi.org/10.5772/intechopen.71686

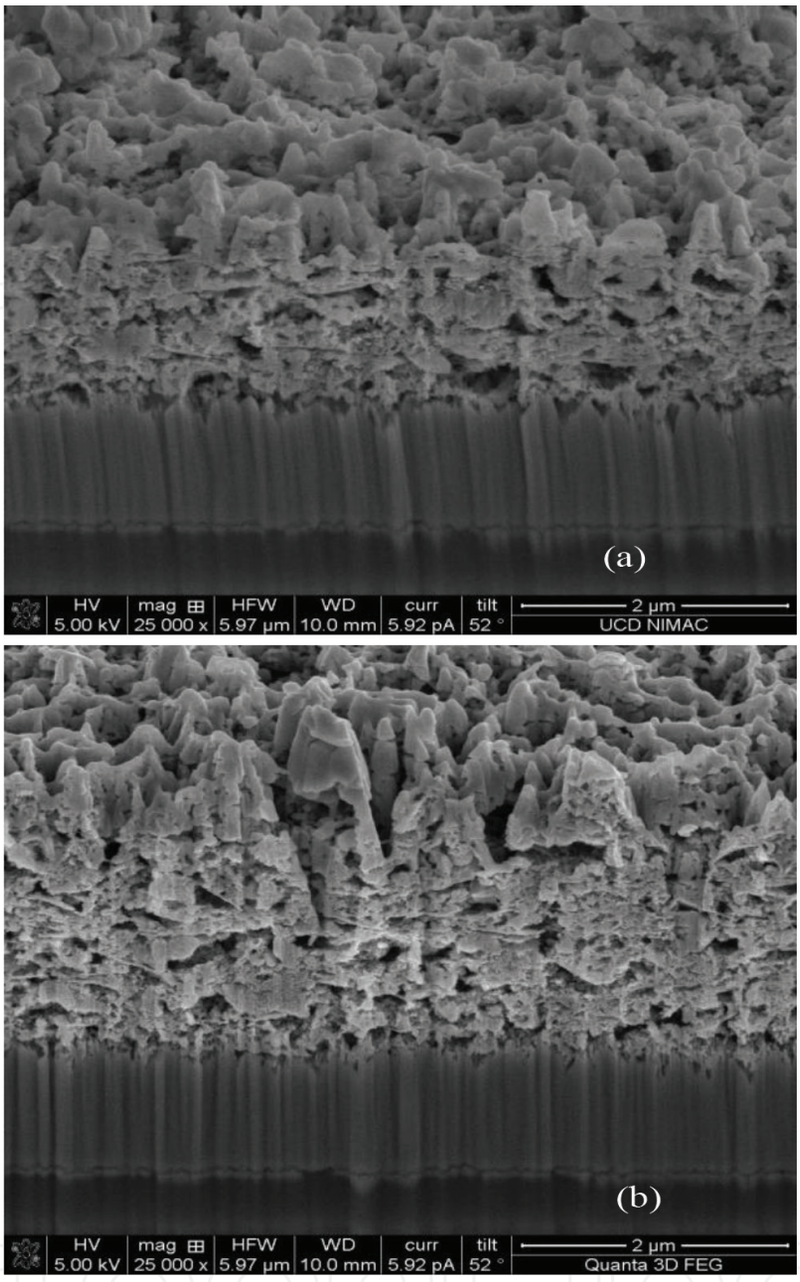

Figure 4. FIB/SEM cross section images of NiO coatings obtained after 5 min sintering using (a) the furnace and (b) the RDS technique. Both coating thicknesses were approximately 2.5 μm. Reprinted from [42] with permission from Elsevier.

2.2. Sintered titanium dioxide (TiO_2) nanoparticles

Since the use of TiO_2 as a photoanode in the fabrication of a DSSC in 1991 by O'Regan and Grätzel [55], many researchers employ TiO_2 for DSSC and other related applications. The phase transformation of TiO_2 coatings is generally carried out using furnace sintering, however, as discussed earlier, it is time consuming. In this section, we will present the use of RDS as viable unconventional sintering technique to convert amorphous TiO_2 to crystalline phase(s). The effect of carbon doping on the resultant coating is also discussed. In this review, the TiO_2 coating of interest with respect to sintering will be that obtained by Dang et al. [56],

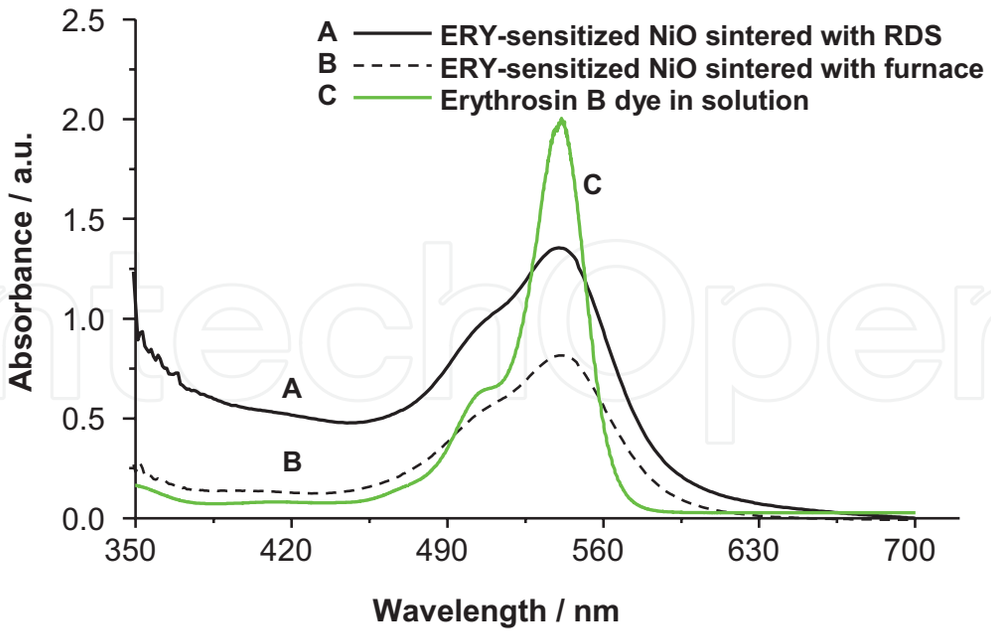

Figure 5. UV-vis absorbance spectra dye sensitized NiO coatings of 1–2 μm thickness (RDS and furnace sintered) and ERY dye in solution. Reprinted from [42] with permission from Elsevier.

Awais et al. [42, 46]/*Reported data* (NiO thickness)	**Treatment time (min)**	**V_{OC} (mV)**	**J_{SC} (mAcm^{-2})**	**FF**	**Efficiency (η)**
RDS treated (~2.5 μm thick)	5	120.00	1.05	36	0.0450
Furnace sintered (~2.5 μm thick)	5	84.00	0.22	25	0.0050
Furnace sintered (~2.5 μm thick)	30	35.29	0.21	26	0.0023
RDS treated (~1–2 μm thick)	5	72.14	0.53	28	0.0118
Furnace sintered (~1–2 μm thick)	5	50.30	0.24	28	0.0037
He et al. [54] (~1 μm thick)	*60*	*83.00*	*0.20*	*27*	*0.0070*
Nattestad et al. [48] (~1.6 μm thick)	*20*	*120.00*	*0.36*	*26*	*0.0110*

Table 1. Photovoltaic performance of RDS and furnace NiO coatings used as photocathode in construction of p-type DSSC (compared with the literature). AM 1.5 solar simulator (*I*: 870 W m^{-2}), 0.5 M LiI and 0.05 M I_2 in propylene carbonate as an electrolyte [52]. Values in italics represent reported literature data.

for example. The following type of coatings are analyzed for their performance: furnace sintered C-doped, RDS treated undoped and C-doped RDS treated.

2.2.1. Comparison of RDS and air furnace treatments of porous TiO_2

TiO_2 coatings were also used to fabricate DSSC electrodes. TiO_2 and carbon-doped TiO_2 were deposited as coatings onto unheated titanium and silicon wafer substrates using a DC closed-field magnetron sputtering system [56]. The C-doped TiO_2 coatings were

http://dx.doi.org/10.5772/intechopen.71686

obtained by introducing low concentrations of carbon dioxide into the argon/oxygen plasma during the sputtering of the metal. The resultant coatings had an amorphous structure and a post-deposition heat treatment is required to convert this amorphous structure into the photoactive crystalline phase(s) of TiO_2. This was achieved using the CAP microwave plasma heat treatment using a nitrogen plasma. During the plasma treatment, the substrate temperature was about 550°C. At this temperature and for treatment times as short as 1 min, 0.25 μm thick coatings converted into the anatase crystalline phase of TiO_2. Further treatments of the coatings at higher temperatures resulted in anatase-to-rutile crystalline phase transformation [56]. As reported earlier for the NiO layers the use of microwave plasma heat treatments facilitated a much more rapid processing compared with furnace heat treatments. It was also observed that the plasma treated TiO_2 coatings also exhibited higher photocurrent density. This is possibly as a result of higher level of surface roughness and consequently a higher available surface area observed for these coatings [56].

As for the plasma treated TiO_2 coatings, C-doped coatings also exhibited a higher roughness when plasma treated compared to furnace treated (**Figure 6**). To investigate the phase transformation efficiency of the two treatment methods as well as the effect of carbon doping, an XRD profile of undoped and C-doped TiO_2 coatings was obtained. As shown in **Figure 7(a)**, anatase phase peaks were observed for coatings treated between 550 and 850°C. As the temperature is increased to 875°C, peaks indicative of the rutile phase could be observed. Interestingly, for the C-doped TiO_2 coatings, the rutile phase can be observed at 750°C (**Figure 7(b)**); thus, it is possible that carbon doping lowered the transitional phase change temperature of anatase to rutile.

In order to evaluate the effect of doping on the efficiency of the TiO_2 coated electrodes, photocurrent density (I_{Ph}) measurements were obtained, as presented in **Table 2**. The highest value

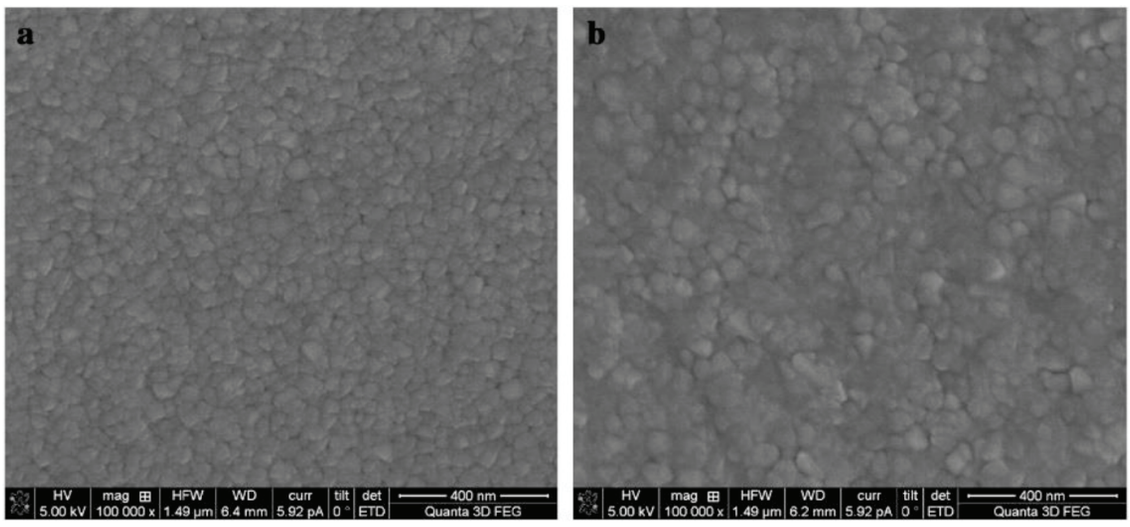

Figure 6. Surface morphology of 2.2% C-doped TiO_2 (a) furnace-treated and (b) MW plasma-treated at 750°C for 3 min. Reprinted from [56] with permission from Elsevier.

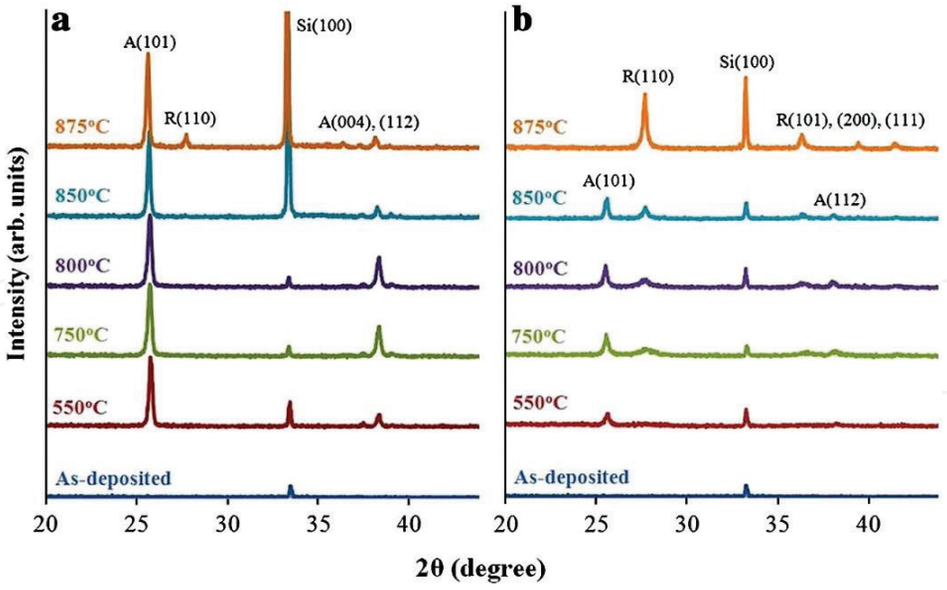

Figure 7. XRD profile of as deposited (a) undoped and (b) 2.2% C-doped TiO_2 upon RDS treatment. Reprinted from [56] with permission from Elsevier.

TiO_2 coatings	Photocurrent density values, I_{Ph} (μA/cm²)
As-deposited (C-doped)	108
Furnace sintered (C-doped)	181
RDS treated (un-doped)	167
RDS treated (C-doped)	216

Table 2. Photocurrent density values for different TiO_2 coatings.

of photocurrent density was obtained for the case of carbon doped plasma treated TiO_2 coatings. There was a 19% increase in the I_{Ph} value in comparison to those treated in the furnace. Possible reasons for the superior performance could be due to the enhanced porosity level of plasma treated coatings, which may have provided more active sites for charge production [56]. A further factor could be that the retention of more doped carbon in the RDS-treated TiO_2 coatings further reduced the band gap of RDS-treated compared to the furnace-treated TiO_2 coatings (See **Figure 8**).

2.3. Conclusion and potential of the RDS sintering technique

RDS-treated NiO coatings were found to exhibit a light-to-current conversion efficiency increase of almost a 10-fold, compared with that obtained for the furnace treated oxide coating. Amongst the likely reasons for the enhanced performance is the smaller grain size, along with the more open structure obtained using the RDS technique.

http://dx.doi.org/10.5772/intechopen.71686

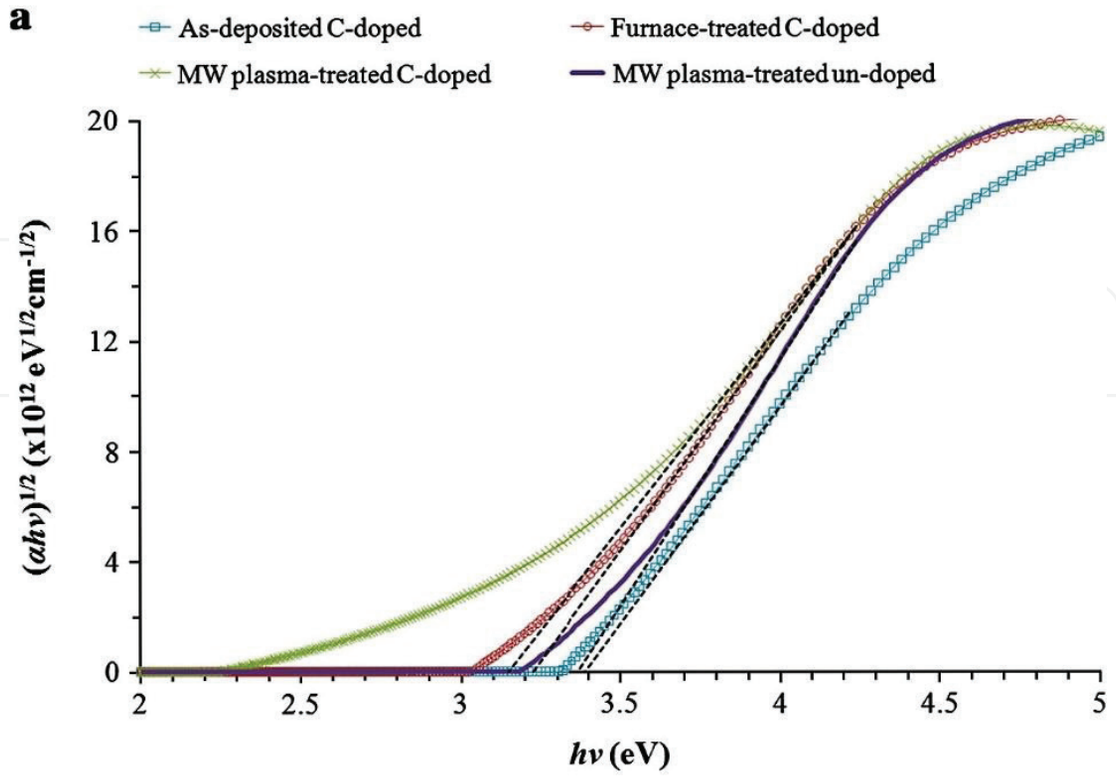

Figure 8. Band gap measurements for as-deposited, furnace treated, RDS treated (2.2% carbon doped) and undoped RDS treated TiO_2 coatings. Reprinted from [56] with permission from Elsevier.

3. Direct porous ceramics growth from metal substrates

In this study, the performance of microwave plasma treatments as a technique for the oxidation of metallic surfaces is investigated. Oxides of titanium formed either on the metal surface or alternatively as TiO_2 coatings (discussed in Section 2.2) have found applications in areas ranging from medical devices (cell attachment), solar cells (light capture), air and water purification, gas sensing, wear protective coatings, etc. [57–62]. This is due to the oxide's photocatalytic, biocompatibility properties, as well as its physical and chemical stability. These properties would depend on the morphology, surface roughness and porosity of the oxides.

Compared to furnace heat treatments, microwave plasma-treated TiO_2 coatings discussed in Section 2.2 possess higher level of surface roughness and hence photoactivity. However, the enhanced surface roughness is still only in the order of a few nanometers and thus, the photoactivity of the resulting coatings is relatively limited [63]. An alternative fabrication method which has been investigated to address this shortcoming is presented in this section.

3.1. RDS oxidation of titanium metal substrates

The plasma treatments were carried out as before using the CAP microwave reactor, in this case using an oxygen discharge [63, 64]. Prior to plasma oxidation, the titanium disc test

substrates were polished to a mirror finish and then solvent cleaned. The oxidized substrates exhibited a white appearance, as shown in **Figure 9**; this is in contrast to the metallic appearance of the non-oxidized titanium metal.

A typical FIB/metallography SEM cross-section image of a RDS treated TiO_2 structure obtained using a focused ion beam (FIB) and metallographic technique for comparison is shown in **Figure 10**. It can be observed that the two sample preparation methods (FIB and metallography) did not alter the porous structure of the ceramics.

3.2. Influence of substrate temperature on the pore structure morphology in a RDS grown oxide-layer

The porosity of the oxide-layer structure was found to generally increase with increase in thickness and treatment temperature (**Figure 11**). Examination of the porous oxide structures indicates that oxide-layers grown at temperature below 880°C exhibits a relatively porous structure, in the upper oxide layer compared to that closer to the metal substrate. Oxides fabricated above 880°C exhibited a further increase in porosity levels throughout the oxide layer. It is well known that α to β phase transformation of titanium occurs at approximately 882°C; this may have influenced porosity distribution observed in the oxide-layers grown on titanium substrates above 880°C [64].

3.3. Comparison of the porosity of sintered TiO_2, air furnace and RDS grown oxide-layer

Figure 12 shows the oxide layer morphology of a RDS and air furnace grown ceramic structures. The structure in **Figure 12(a)** was obtained after 5-hours furnace treatment in air and its thickness was found to be 4.17 μm. In contrast, after treatment in an oxygen microwave plasma for 10 min, the thickness obtained was 6.96 μm (**Figure 12(b)**). It can be observed that the oxide-layer obtained using the microwave plasma oxidation exhibited a relatively

Figure 9. Photograph of oxide-layer formed on the 25-mm diameter titanium disc using microwave plasma and air furnace. Reprinted from [64] with permission from Elsevier.

http://dx.doi.org/10.5772/intechopen.71686

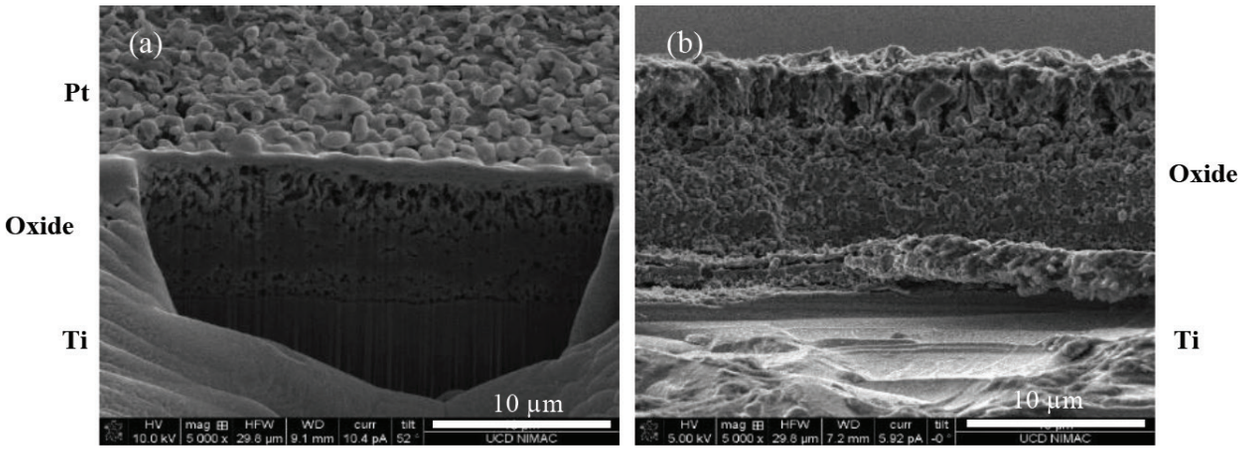

Figure 10. SEM images of oxide cross-section prepared using the FIB (a) and metallographic technique (b). The images were obtained using an FEI Quanta 3D FEG DualBeam system. The average oxide-layer thickness for both techniques is 9.89 µm. (Note a 52° tilt angle is used for the FIB image.) Reprinted from [64] with permission from Elsevier.

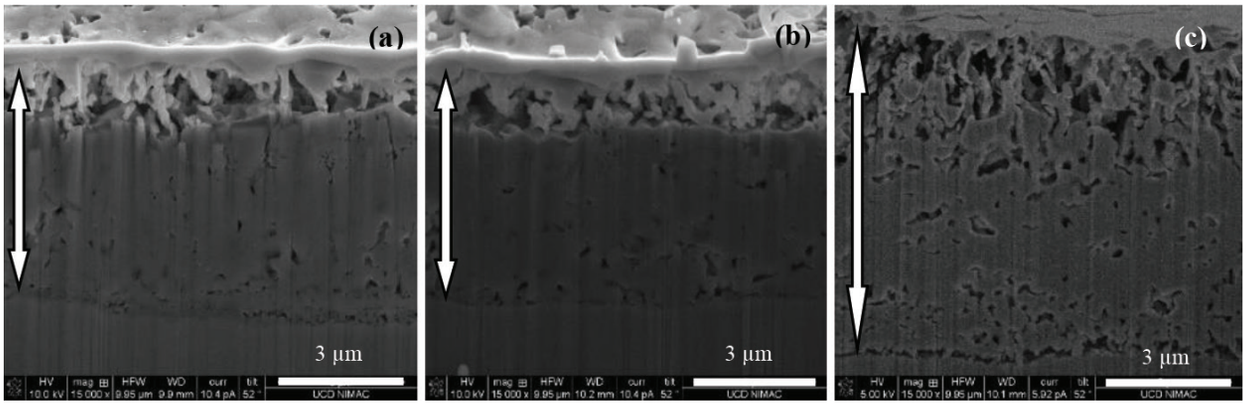

Figure 11. Oxide-layers (demonstrated using the arrows), which were grown on titanium substrates at temperature: (a) 855°C, (b) 880°C and (c) 910°C showing porosity distribution. Note the increased porosity obtained at the higher oxidation temperature. Reprinted from [64] with permission from Elsevier.

rough morphology, with large grains. In contrast, the slower growing oxide formed using the furnace oxidation exhibited a much denser morphology with little or no porosity observed. A possible reason for the increased porosity obtained for the RDS treatments is a result of a preferential grain growth in specific directions due to a van der Drift type of competition with increasing thickness of oxide layer [64].

To conclude it is interesting to compare the morphology of two TiO_2 oxide layers obtained as part of this study as shown in **Figure 13**. **Figure 13(a)** was obtained by oxidation of metal oxide nanoparticles and **Figure 13(b)** by the oxidation of the titanium metal. Both were obtained using the microwave plasma treatments. It is clear from **Figure 13** that the sintering of the TiO_2 nanoparticles yields a much more homogeneous oxide pore structure. Its fabrication, however, involves two steps (spray deposition and sintering), compared with the single microwave plasma oxidation step. Both treatments, however, demonstrate the flexibility of the microwave plasma treatments.

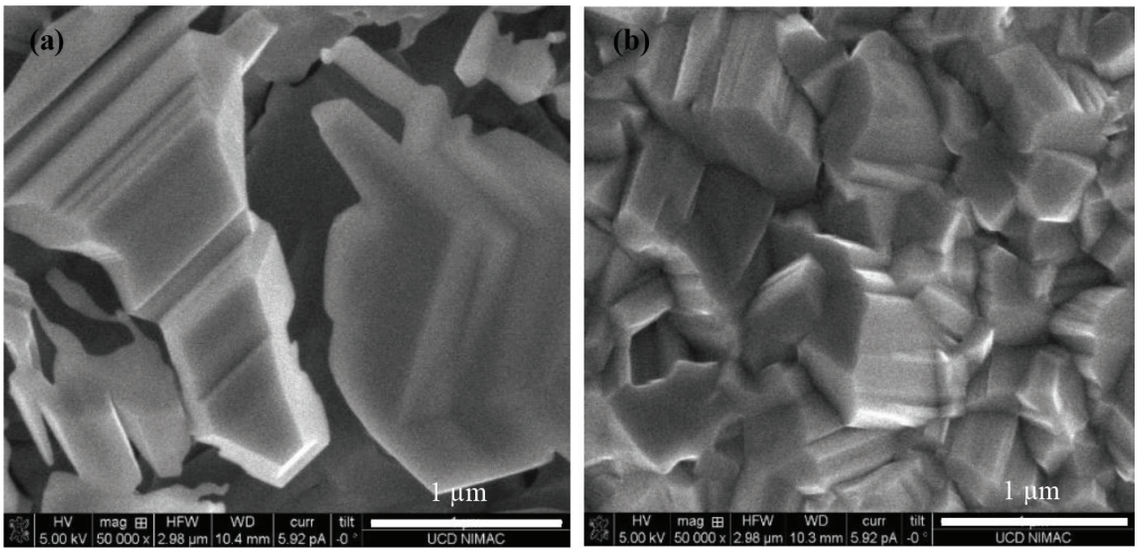

Figure 12. Typical SEM images of oxide-layers grown using a RDS (a); and air furnace (b), demonstrating differences in the grain structure obtained (samples both prepared at a treatment temperature of 790°C). Reprinted from [64] with permission from Elsevier.

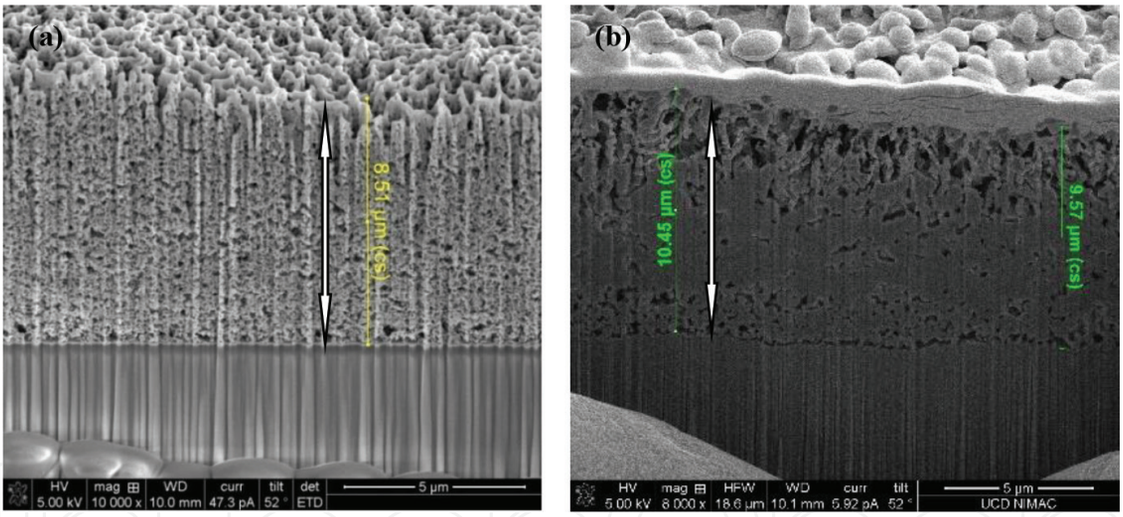

Figure 13. FIB cross-sections of an 8.5 µm thick TiO_2 coating (a) fabricated by sintering TiO_2 nanoparticles. The FIB cross section (b) shows a 10.45 µm TiO_2 oxide-layer obtained by oxidizing the Cp titanium metal (reprinted from [64] with permission from Elsevier).

4. Conclusions

The use of microwave plasma treatments has been reviewed both for sintering nanoparticles (referred to as rapid discharge sintering (RDS), as a thermal processing route for crystalline phase changes, as well as for the oxidation of metal surfaces. For the fabrication of porous ceramics, the plasma treatments have the advantage of being rapid and flexible allowing for the tailoring and control of pore structures with processing conditions. Compared to the conventional methods such as air furnace treatment, the plasma treatments were demonstrated

to yield improved results in terms of shorter treatment time, lower energy requirement and enhanced performance. The latter was demonstrated in the case of metal oxide layers (NiO and TiO_2), when evaluated for use in solar energy applications.

Author details

Emmanuel J. Ekoi[1]*, Muhammad Awais[2] and Denis P. Dowling[1]

*Address all correspondence to: emmanuel.ekoi@ucdconnect.ie

1 School of Mechanical and Materials Engineering, University College Dublin, Dublin 4, Ireland

2 Department of Industrial Engineering, Taibah University, Medina, Saudi Arabia

References

[1] Clark DE, Folz DC, West JK. Processing materials with microwave energy. Materials Science and Engineering: A. 2000;**287**(2):153-158

[2] Das S, Mukhopadhyay AK, Datta S, Basu D. Prospects of microwave processing: An overview. Bulletin of Materials Science. 2009;**32**(1):1-13

[3] Sutton WH. Microwave processing of ceramics-an overview. In: MRS Proceedings. Vol. 269. Cambridge University Press; Cambridge, UK, 1992. p. 3

[4] Agrawal D. Microwave sintering of metal powders. In: Chang I, Zhao Y, editors. Advances in Powder Metallurgy. Woodhead Publishing Ltd; Sawston, UK, 2013. p. 361-379

[5] Thostenson ET, Chou TW. Microwave processing: Fundamentals and applications. Composites Part A: Applied Science and Manufacturing. 1999;**30**(9):1055-1071

[6] Roy R, Agrawal D, Cheng J, Gedevanishvili S. Full sintering of powdered-metal bodies in a microwave field. Nature. 1999;**399**(6737):668-670

[7] Sethi G, Upadhyaya A, Agrawal D. Microwave and conventional sintering of premixed and prealloyed Cu-12Sn bronze. Science of Sintering. 2003;**35**(2):49-65

[8] Takayama S, Saiton Y, Sato M, Nagasaka T, Muroga T, Ninomiya Y. Microwave sintering for metal powders in the air by non-thermal effect. In: Proceedings of the 9th Conference on Microwave and High Frequency Heating; 2003. pp. 369-372

[9] Gupta M, Wong WLE. Enhancing overall mechanical performance of metallic materials using two-directional microwave assisted rapid sintering. Scripta Materialia. 2005; **52**(6):479-483

[10] Saitou K. Microwave sintering of iron, cobalt, nickel, copper and stainless steel powders. Scripta Materialia. 2006;**54**(5):875-879

[11] Agrawal D. Microwave sintering of ceramics, composites and metallic materials, and melting of glasses. Transactions of the Indian Ceramic Society. 2006;**65**(3):129-144

[12] Lieberman MA, Lichtenberg AJ. Principles of Plasma Discharges and Materials Processing. John Wiley & Sons; New Jersey, USA, 2005

[13] Möller W. Fundamentals of Plasma Physics. University of Technology Dresden; Dresden, Germany, 2014

[14] Conrads H, Schmidt M. Plasma generation and plasma sources. Plasma Sources Science and Technology. 2000;**9**(4):441

[15] Bellan PM. Fundamentals of Plasma Physics. Cambridge University Press; Cambridge, UK, 2008

[16] Go D. Gaseous Ionization and Ion Transport: An Introduction to Gas Discharges. Department of Aerospace and Mechanical Engineering University of Notre Dame; Indiana, USA, 2012

[17] Moisan M, Barbeau C, Claude R, Ferreira CM, Margot J, Paraszczak J, et al. Radio frequency or microwave plasma reactors? Factors determining the optimum frequency of operation. Journal of Vacuum Science & Technology B: Microelectronics and Nanometer Structures Processing, Measurement, and Phenomena. 1991;**9**(1):8-25

[18] Kabouzi Y, Calzada MD, Moisan M, Tran KC, Trassy C. Radial contraction of microwave-sustained plasma columns at atmospheric pressure. Journal of Applied Physics. 2002;**91**(3):1008-1019

[19] Tendero C, Tixier C, Tristant P, Desmaison J, Leprince P. Atmospheric pressure plasmas: A review. Spectrochimica Acta Part B: Atomic Spectroscopy. 2006;**61**(1):2-30

[20] Pleuler E, Wild C, Füner M, Koidl P. The CAP-reactor, a novel microwave CVD system for diamond deposition. Diamond and Related Materials. 2002;**11**(3):467-471

[21] McConnell ML, Dowling DP, Pope C, Donnelly K, Ryder AG, O'Connor GM. High pressure diamond and diamond-like carbon deposition using a microwave CAP reactor. Diamond and Related Materials. 2002;**11**(3):1036-1040

[22] Kakizaka S, Sakamoto T, Matsuura H, Akatsuka H. Titanium oxidation by microwave discharge oxygen plasma and relationship with plasma parameters. Journal of Advanced Oxidation Technologies. 2007;**10**(2):253-259

[23] Ganguli A, Tarey RD. Understanding plasma sources. Current Science. 2002;**83**(3):279-290

[24] Toumanov IN. Plasma and High Frequency Processes for Obtaining and Processing Materials in the Nuclear Fuel Cycle. Nova Publishers; New York, USA, 2003. p. 64

[25] Eliasson B, Kogelschatz U. Nonequilibrium volume plasma chemical processing. IEEE Transactions on Plasma Science. 1991;**19**(6):1063-1077

[26] Lu G, Bernasek SL, Schwartz J. Oxidation of a polycrystalline titanium surface by oxygen and water. Surface Science. 2000;**458**(1):80-90

[27] Del Pino AP, Serra P, Morenza JL. Oxidation of titanium through Nd: YAG laser irradiation. Applied Surface Science. 2002;**197**:887-890

[28] Gemelli E, Camargo NHA. Oxidation kinetics of commercially pure titanium. Matéria (Rio de Janeiro). 2007;**12**(3):525-531

[29] Li LH, Kong YM, Kim HW, Kim YW, Kim HE, Heo SJ, Koak JY. Improved biological performance of Ti implants due to surface modification by micro-arc oxidation. Biomaterials. 2004;**25**(14):2867-2875

[30] Diefenbeck M, Mückley T, Schrader C, Schmidt J, Zankovych S, Bossert J, et al. The effect of plasma chemical oxidation of titanium alloy on bone-implant contact in rats. Biomaterials. 2011;**32**(32):8041-8047

[31] Kofstad P, Hauffe K, Kjollesdal H. Investigation on the oxidation mechanism of titanium. Acta Chemica Scandinavica. 1958;**12**(2):239-266

[32] Orii Y, Masumoto H, Honda Y, Anada T, Goto T, Sasaki K, Suzuki O. Enhancement of octacalcium phosphate deposition on a titanium surface activated by electron cyclotron resonance plasma oxidation. Journal of Biomedical Materials Research Part B: Applied Biomaterials. 2010;**93**(2):476-483

[33] Agrawal DK. Microwave processing of ceramics. Current Opinion in Solid State and Materials Science. 1998;**3**(5):480-485

[34] Bykov YV, Rybakov KI, Semenov VE. High-temperature microwave processing of materials. Journal of Physics D: Applied Physics. 2001;**34**(13):R55

[35] Campana DM, Ubal S, Giavedoni MD, Saita FA. A deeper insight into the dip coating process in the presence of insoluble surfactants: A numerical analysis. Physics of Fluids. 2011;**23**(5):052102

[36] Bennett CEG, McKinnon NA, Williams LS. Sintering in gas discharges. Nature. 1968;**217** (5135):1287-1288

[37] Twomey B, Breen A, Byrne G, Hynes A, Dowling DP. Rapid discharge sintering of nickel–diamond metal matrix composites. Journal of Materials Processing Technology. 2011;**211**(7):1210-1216

[38] Breen AP, Twomey B, Byrne G, Dowling DP. Comparison between microwave and microwave plasma sintering of nickel powders. In: Materials Science Forum. Vol. 672. Trans Tech Publications; Zürich, Switzerland, 2011. p. 289-292

[39] Awais M, Dini D, Vos JG, Dowling DP. Nickel oxide photocathodes prepared using rapid discharge sintering for p-type dye-sensitized solar cells. Journal of the Chemical Society of Pakistan. 2016;**38**(4):615-615

[40] Awais M, Gibson E, Vos JG, Dowling DP, Hagfeldt A, Dini D. Fabrication of efficient NiO photocathodes prepared via RDS with novel routes of substrate processing for p-type dye-sensitized solar cells. ChemElectroChem. 2014;**1**(2):384-391

[41] Gibson EA, Awais M, Dini D, Dowling DP, Pryce MT, Vos JG, et al. Dye sensitised solar cells with nickel oxide photocathodes prepared via scalable microwave sintering. Physical Chemistry Chemical Physics. 2013;**15**(7):2411-2420

[42] Awais M, Rahman M, MacElroy JD, Dini D, Vos JG, Dowling DP. Application of a novel microwave plasma treatment for the sintering of nickel oxide coatings for use in dye-sensitized solar cells. Surface and Coatings Technology. 2011;**205**:S245-S249

[43] Sato H, Minami T, Takata S, Yamada T. Transparent conducting p-type NiO thin films prepared by magnetron sputtering. Thin Solid Films. 1993;**236**(1):27-31

[44] Lu YM, Hwang WS, Yang JS, Chuang HC. Properties of nickel oxide thin films deposited by RF reactive magnetron sputtering. Thin Solid Films. 2002;**420**:54-61

[45] Odobel F, Le Pleux L, Pellegrin Y, Blart E. New photovoltaic devices based on the sensitization of p-type semiconductors: Challenges and opportunities. Accounts of Chemical Research. 2010;**43**(8):1063-1071

[46] Muhammad Awais, Denis P. Dowling, Franco Decker, Danilo Dini. Electrochemical Characterization of Nanoporous Nickel Oxide Thin Films Spray-Deposited onto Indium-Doped Tin Oxide for Solar Conversion Scopes. Advances in Condensed Matter Physics, vol. 2015, Article ID 186375, 18 pages, 2015. DOI:10.1155/2015/186375

[47] Nakasa A, Usami H, Sumikura S, Hasegawa S, Koyama T, Suzuki E. A high voltage dye-sensitized solar cell using a nanoporous NiO photocathode. Chemistry Letters. 2005; **34**(4):500-501

[48] Nattestad A, Ferguson M, Kerr R, Cheng YB, Bach U. Dye-sensitized nickel (II) oxide photocathodes for tandem solar cell applications. Nanotechnology. 2008;**19**(29):295304

[49] Tachibana Y, Hara K, Sayama K, Arakawa H. Quantitative analysis of light-harvesting efficiency and electron-transfer yield in ruthenium-dye-sensitized nanocrystalline TiO_2 solar cells. Chemistry of Materials. 2002;**14**(6):2527-2535

[50] Grätzel M. Conversion of sunlight to electric power by nanocrystalline dye-sensitized solar cells. Journal of Photochemistry and Photobiology A: Chemistry. 2004;**164**(1):3-14

[51] McConnell RD. Assessment of the dye-sensitized solar cell. Renewable and Sustainable Energy Reviews. 2002;**6**(3):271-293

[52] Awais M. Deposition and evaluation of nickel oxide coatings for dye-sensitized solar cell application [Doctoral dissertation]. University College Dublin; Dublin, Ireland, 2011

[53] Twomey B, Breen A, Byrne G, Hynes A, Dowling D. Plasma power can slash small run sintering times. Metal Powder Report. 2010;**65**(2):10-13

[54] He J, Lindström H, Hagfeldt A, Lindquist SE. Dye-sensitized nanostructured tandem cell-first demonstrated cell with a dye-sensitized photocathode. Solar Energy Materials and Solar Cells. 2000;**62**(3):265-273

[55] O'Regan B, Grätzel M. A low-cost, high-efficiency solar cell based on dye-sensitized colloidal TiO_2 films. Nature. 1991;**353**(6346):737-740

[56] Dang BH, Rahman M, MacElroy D, Dowling DP. Conversion of amorphous TiO_2 coatings into their crystalline form using a novel microwave plasma treatment. Surface and Coatings Technology. 2011;**205**:S235-S240

[57] Liu X, Chu PK, Ding C. Surface modification of titanium, titanium alloys, and related materials for biomedical applications. Materials Science and Engineering: R: Reports. 2004;**47**(3):49-121

[58] Fujishima A, Honda K. Electrochemical photolysis of water at a semiconductor electrode. Nature. 1972;**238**(5358):37-38

[59] Hanaor DA, Sorrell CC. Sand supported mixed-phase TiO_2 photocatalysts for water decontamination applications. Advanced Engineering Materials. 2014;**16**(2):248-254

[60] Kuciauskas D, Freund MS, Gray HB, Winkler JR, Lewis NS. Electron transfer dynamics in nanocrystalline titanium dioxide solar cells sensitized with ruthenium or osmium polypyridyl complexes. The Journal of Physical Chemistry B. 2001;**105**(2):392-403

[61] Boccaccini AR, Karapappas P, Marijuan JM, Kaya C. TiO_2 coatings on silicon carbide and carbon fibre substrates by electrophoretic deposition. Journal of Materials Science. 2004;**39**(3):851-859

[62] Shen GX, Chen YC, Lin CJ. Corrosion protection of 316 L stainless steel by a TiO_2 nanoparticle coating prepared by sol–gel method. Thin Solid Films. 2005;**489**(1):130-136

[63] Dang BH, Rahman M, MacElroy D, Dowling DP. Evaluation of microwave plasma oxidation treatments for the fabrication of photoactive un-doped and carbon-doped TiO_2 coatings. Surface and Coatings Technology. 2012;**206**(19):4113-4118

[64] Ekoi EJ, Stallard C, Reid I, Dowling DP. Tailoring oxide-layer formation on titanium substrates using microwave plasma treatments. Surface and Coatings Technology. 2017; **325**:299-307

IntechOpen